Acta Crystallographica Section D
Biological Crystallography
ISSN 0907-4449

Structure of a new neurotoxin from the scorpion *Buthus martensii* Karsch at 1.76 Å

Xiao-Lin He, Jun-Peng Deng, Miao Wang, Ying Zhang and Da-Cheng Wang*

Institute of Biophysics, Chinese Academy of Sciences, Beijing 100101, People's Republic of China

Correspondence e-mail: wdc@pewdc.ibp.ac.cn

Received 15 July 1999
Accepted 10 November 1999

PDB Reference: BmK M2, 1chz.

A new neurotoxin BmK M2, toxic to both mammals and insects, with the strongest toxicity in the BmK toxin series, has been purified from the Chinese scorpion *Buthus martensii* Karsch and crystallized with MPD at pH 7.5. The crystals are orthorhombic, belonging to space group $P2_12_12_1$, with unit-cell parameters $a = 36.64$, $b = 36.95$, $c = 37.23$ Å. The structure was solved by molecular replacement and refined to $R = 0.186$ for all reflections to a resolution of 1.76 Å. The whole sequence (64 residues) of BmK M2 was determined by crystallographic analysis based on high-resolution data and the homologous model of BmK M8. The refined BmK M2 structure shows a non-proline *cis* peptide bond between Pro9 and His10 which enables the C-terminal segment to adopt a conformation different to that of the weak toxin BmK M8. Recently, a mutation analysis had suggested that both the tenth residue and the C-terminus play key roles in receptor binding. Therefore, these features may be related to the binding selectivity of the group III α-like toxins. The charge changes of residues 8, 10, 18, 28, 55 and 59 from neutral or negative to positive or neutral, which leads to a positive electrostatic potential surface, may be responsible for the high toxicity of BmK M2.

1. Introduction

Scorpion venom contains a cocktail of neurotoxins. These toxins bind to different receptors on the membrane of neuromuscular cells and cause serious symptoms (Rochat *et al.*, 1979). Those toxins binding to the sodium channel were classified into α- and β-types according to their behaviour of inhibiting or deferring the sodium current (Couraud *et al.*, 1982). The α-toxins defer the inactivation of the sodium current and bind to the so-called receptor site 3 on the sodium channel, while the β-toxins inhibit the activation of the sodium current and bind to receptor site 4 (for reviews, see Gordon *et al.*, 1997, 1998). We now know that the α-toxins are mostly derived from the scorpion venoms of the Old World (Eurasia and Africa). The Chinese scorpion *B. martensii* Karsch (BmK) is a representative species in East Asia. Despite the serious symptoms caused by scorpion envenomation in other parts of the world (*e.g.* Africa), the whole body and especially the tail of scorpions has been used as a traditional medicine in China for more than 1000 years. In order to explore the biological basis of the pharmaceutical property and to understand the molecular mechanism of toxin–receptor binding, a series of α-toxins have been isolated, characterized and cloned from the scorpion BmK in our laboratory (Luo *et al.*, 1997; Xiong *et al.*, 1997, 1999; Deng *et al.*, 1996; Hu *et al.*, 1989; Li, Wang *et al.*,

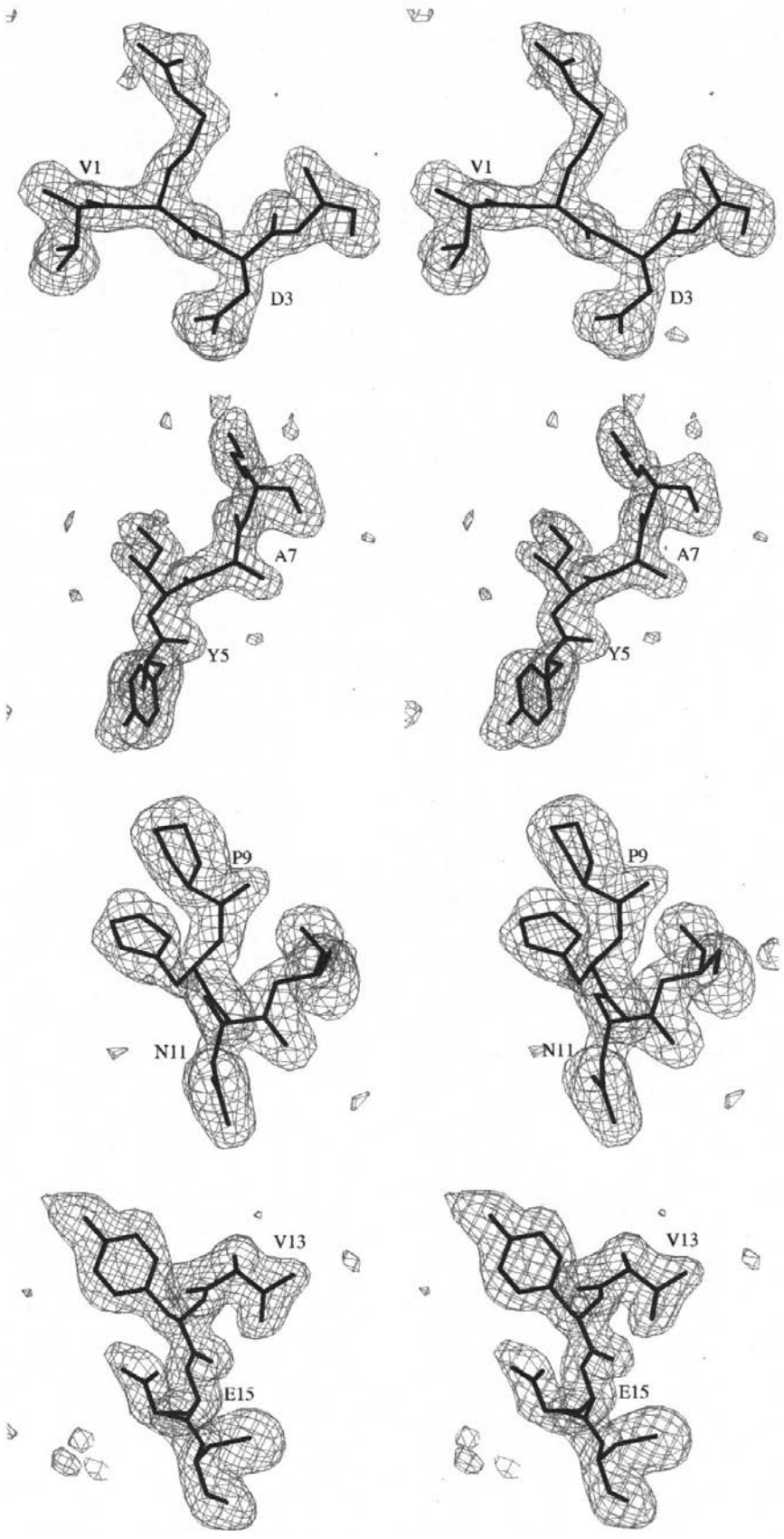

Figure 1
The omit $F_o - F_c$ electron-density map of sets of four residues contoured at 2.0σ: residues 1–16.

1995). Based on these, the crystallographic investigation of some significant BmK neurotoxins has been intensively undertaken in recent years. Despite the availability of the crystal structures of AaH II (Fontecilla-Camps *et al.*, 1988; Housset *et al.*, 1994) and CsE V3 (Almassy *et al.*, 1983; Zhao *et al.*, 1992), which established the representative structural models of α-toxins and β-toxins, respectively, the binding process of scorpion toxins and their structural determinants for animal specificity and bioactivity are yet to be elucidated. To further address the unsolved problems, we found three bioactivity-variant toxins, BmK M1, BmK M4 and BmK M8, from the scorpion BmK (Li *et al.* 1999; He *et al.*, 1999; Li *et al.*, 1996; Jin *et al.*, 1993; Li, Liu *et al.*, 1995). Their relative activities are 13.5:2.5:1, which interestingly corresponds to their respective pI values ranging from basic to acidic. Such positive correlation between toxicity and basicity has also been observed by Watt & Simard (1984) for toxins purified from the North American scorpion *Centruroides sculpturatus* Ewing. Therefore, this toxin series form a valuable system for studying structure–function relationships. The three BmK crystal structures were solved in succession. The structure of BmK M8 revealed that the presence of negative electrostatic potentials on a surface (face *B*) resulting from substitution by acidic residues are relevant to the extremely weak toxicity of the toxin (Li *et al.*, 1996). The structures of BmK M1 and BmK M4 provided information on the structural basis of the receptor binding-site specificity, with a *cis* peptide-bond-mediated mechanism for the group III α-like toxins (He *et al.*, 1999). Recently, in addition to the BmK series described above, a new toxin component BmK M2 was isolated which was toxic to both mammals and insects and possessed the strongest toxic activity to mice (LD_{50} = 0.5 mg kg^{-1}) and also had the most alkaline isoelectric point (pI = 9.44; Deng *et al.*, 1996). The structural analysis of BmK M2, reported here, revealed some determinants of these characteristics. Moreover, the amino-acid sequence of BmK M2 was unknown. Therefore, the successful structural solution of BmK M2 starting from a homologous model of BmK M8 provided some experience on the structural analysis of homologous molecules through crystallographic sequencing.

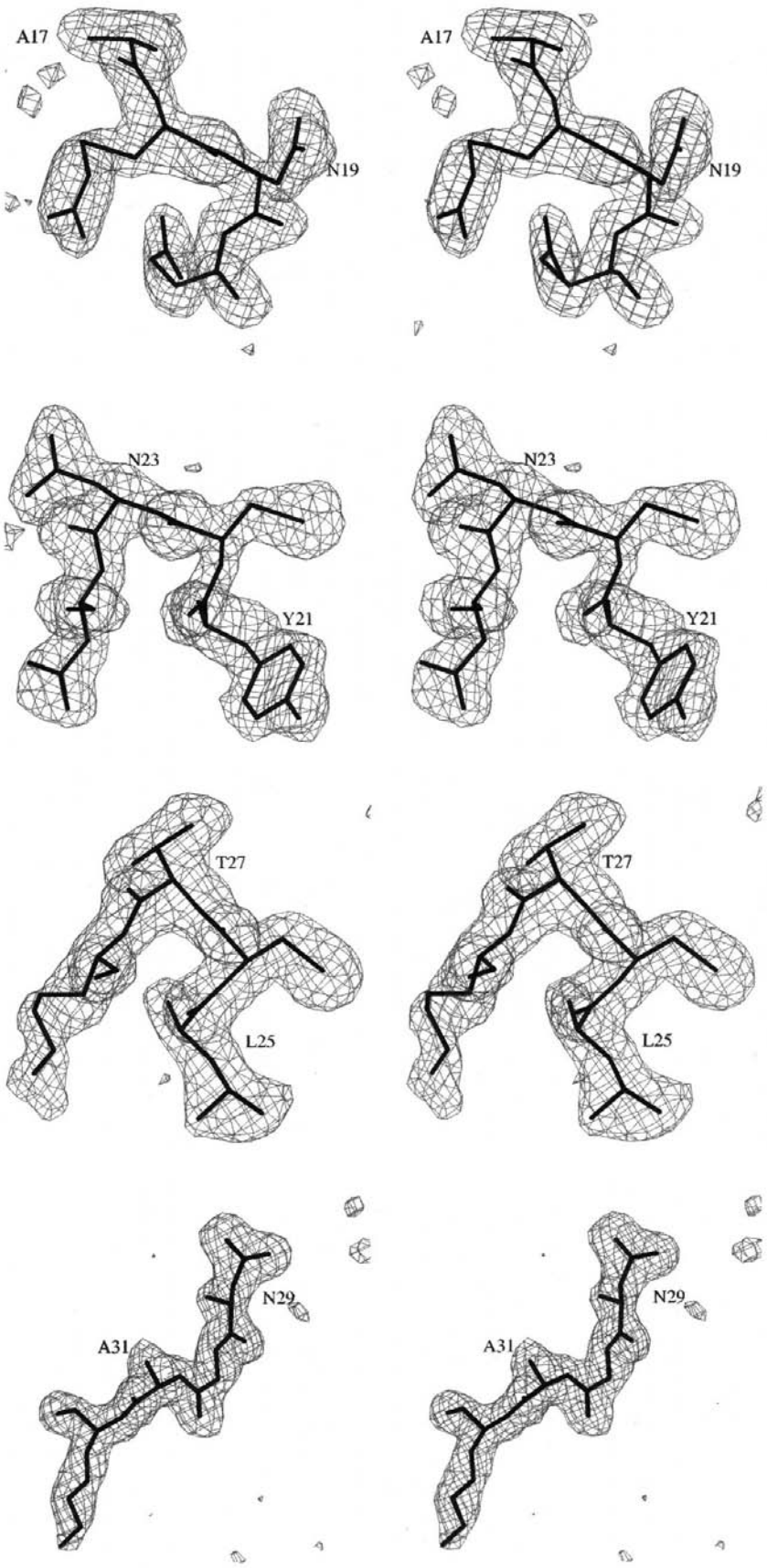

Figure 2
The omit $F_o - F_c$ electron-density map of sets of four residues contoured at 2.0σ: residues 17–32.

2. Experimental

2.1. Purification, crystallization and data collection

The details of the purification of toxin BmK M2 from the venom of *B. martensii* Karsch have been described previously (Deng *et al.*, 1996). One gel-filtration step and one cation-exchange chromatography step were carried out. The crude venom was applied to a Sephadex G50 column. The second peak was pooled, concentrated and then applied to an sp-Sephadex G25 column and washed with phosphate-buffered NaCl at pH 6.7. The eighth peak, corresponding to the second most plentiful component in BmK venom, was collected, desalted and lyophilized. It was characterized to be the most potent BmK toxin to mice and also had anti-insect toxicity.

For crystallization, the purified BmK M2 powder was dissolved in 10 m*M* acetic acid at a concentration of 10 mg ml^{-1}. Crystals were obtained at room temperature by vapour diffusion using the hanging-drop technique. The drops were formed by mixing 3 µl of protein solution with 3 µl of a well solution composed of 65–70% MPD, 0.1 *M* Tris pH 7.5 and 5% dioxane. These drops were equilibrated against a reservoir filled with 500 µl well solution. Crystals appeared after a few days and grew to dimensions of 0.6 × 0.2 × 0.1 mm. They belong to the orthorhombic space group $P2_12_12_1$, with unit-cell parameters $a = 36.64$, $b = 36.95$, $c = 37.23$ Å. The Matthews coefficient was 1.83, assuming that the molecular weight is the same as that of BmK M8 and that there is one molecule per asymmetric unit. Intensity data were collected to a resolution of 1.76 Å from one crystal on a Siemens X-200B area detector, using Cu $K\alpha$ monochromated radiation produced by a Rigaku RU-200 rotating-anode X-ray generator. A total of 11 634 reflections were collected, scaled and merged using the program *XENGEN* (Howard *et al.*, 1987) into a set of 5066 unique reflections with $R_{\rm merge} = 10.0\%$. The completeness was 90.0% to 1.76 Å. The $R_{\rm merge}$ and completeness in the highest resolution shell (1.82–1.76 Å) were 0.34 and 55.3%, respectively.

2.2. Structure determination and refinement

2.2.1. Molecular replacement. The structure of BmK M2 was solved using the molecular-replacement method with the homologous structure of BmK M8 (Li *et al.*, 1996) as the search model. The coordinates

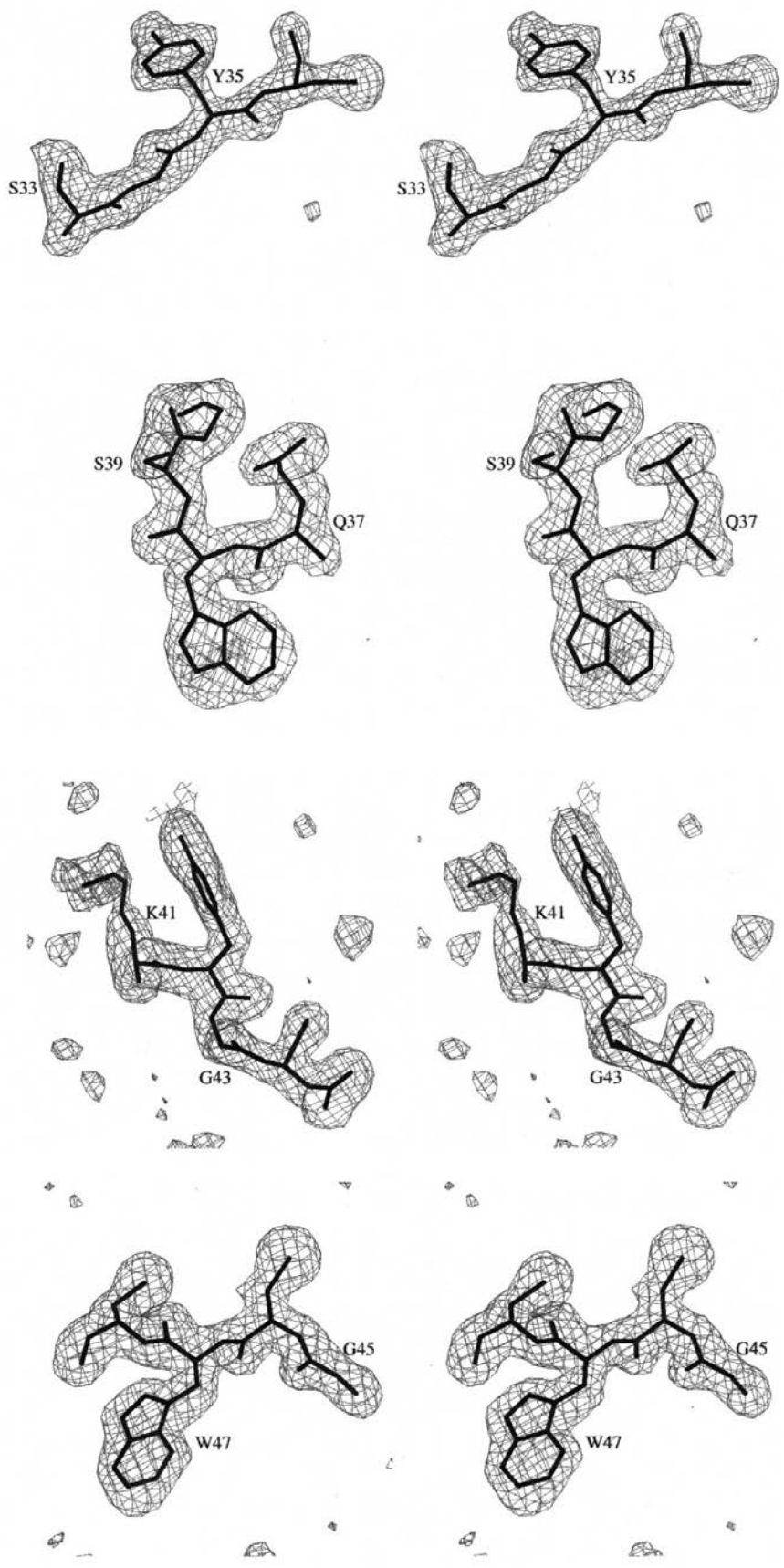

Figure 3
The omit $F_o - F_c$ electron-density map of sets of four residues contoured at 2.0σ: residues 33–48.

(reference 1snb) in the Protein Data Bank (Bernstein *et al.*, 1977) were used as the initial model for the rotation search. All the water molecules were discarded and the temperature factors of all remaining atoms were fixed at 20.0 Å^2. The rotation search was performed in Patterson real space according to the procedure implemented in *X-PLOR* (Brünger *et al.*, 1987). The Patterson of the model was computed in a *P*1 cell (60 × 60 × 40 Å). The data were restricted to the resolution range 10–3.5 Å. The 500 most intense Patterson peaks with a vector length between 10 and 30 Å were selected and a product function was computed at intervals of 5° on an angular grid (θ_1 = 0–360°, θ_2 = 0–90°, θ_3 = 0–180°; Rossman & Blow, 1962). The 100 best solutions were then filtered by the Patterson-correlation (PC) refinement procedure (Brünger, 1990) to provide one unique independent solution (16.0, 205.2, 82.3°) corresponding to the first solution of the rotation search. The best translation solution occurred at (13.86, 7.46, 3.85 Å). The rotated–translated model gave an *R* value of 46.8% for data in the resolution range 10–3.5 Å. Checking the packing in the unit cell with *TURBO-FRODO* (Roussel *et al.*, 1990) found no conflict between the main chains.

2.2.2. Crystallographic refinement. The model was rebuilt with *TURBO-FRODO* (Roussel *et al.*, 1990) and refined with *X-PLOR* (Brünger *et al.*, 1987). No data truncation was applied in the refinement, as suggested by Dodson *et al.* (1996). 10% of the data was set aside in order to calculate the free *R* factor (Kleywegt & Brünger, 1996). After a rigid-body refinement, the *R* value dropped to 0.378 and $R_{\rm free}$ was 0.452 for the data in the resolution range 10–3 Å. The model was then refined by simulated annealing with the slow-cooling protocol provided in *X-PLOR* using data in the resolution range 10–2.5 Å. A starting temperature of 3000 K was gradually decreased to 300 K in stages of 25 K, during which 50 0.005 ps molecular-dynamics steps were run. This process was followed by minimization. At this stage, the *R* factor and $R_{\rm free}$ were 0.224 and 0.287, respectively. Using the 10–1.76 Å data, $2F_o - F_c$ and $F_o - F_c$ electron-density maps were calculated and examined with *TURBO-FRODO* (Roussel *et al.*, 1990). The refinement was completed by alternating between manual

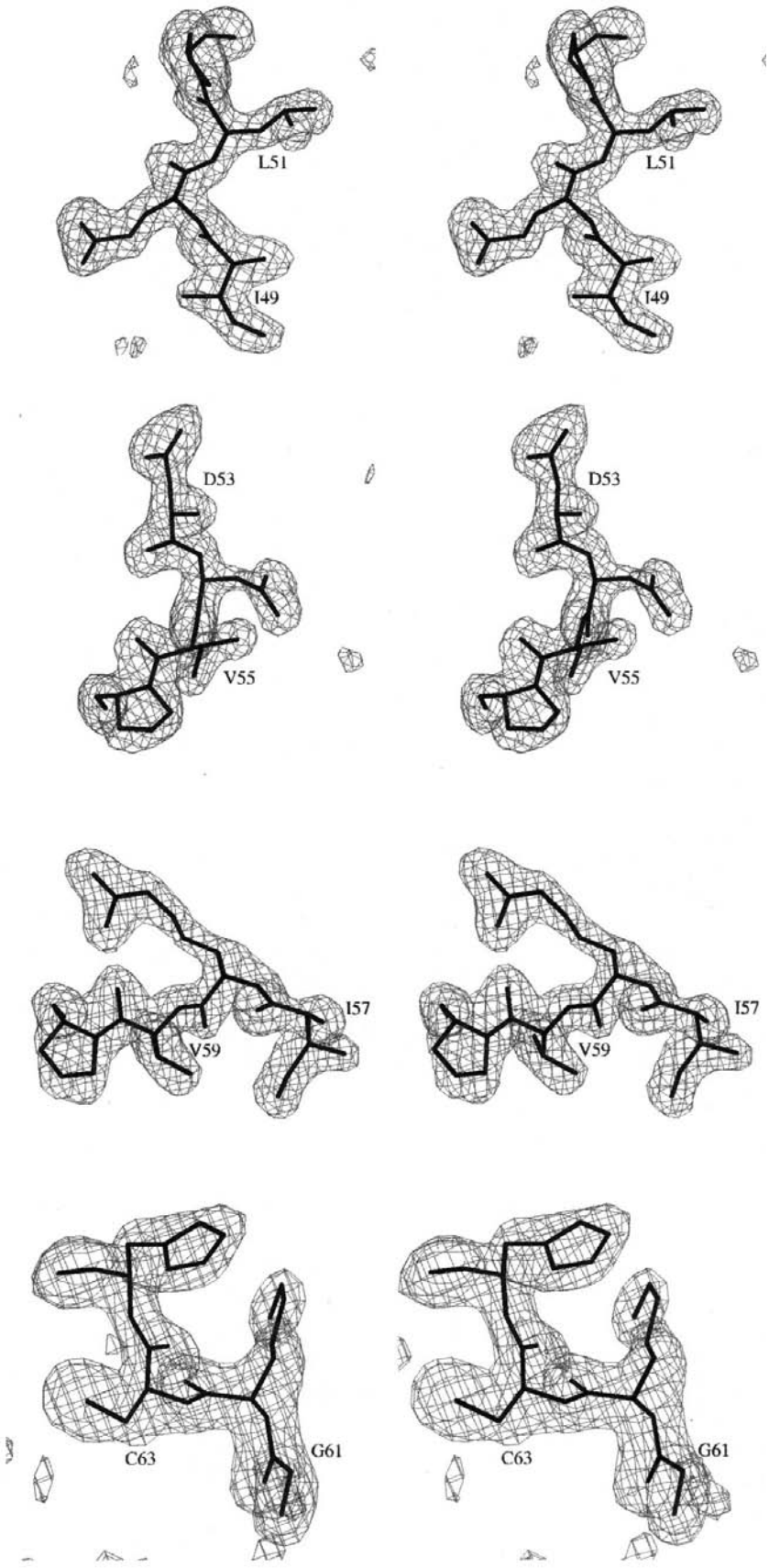

Figure 4
The omit $F_o - F_c$ electron-density map of sets of four residues contoured at 2.0σ: residues 49–64.

rebuilding and minimization using data in the resolution range 20–1.76 Å. Restrained isotropic temperature factors were applied and 89 water molecules were included. Most of the water molecules were located automatically by waterpicking with *X-PLOR*.

2.3. Crystallographic sequencing

The sequence of BmK M2 was unknown when its structural analysis was undertaken. Using the structure of BmK M8 as a homologous model, we discerned the whole sequence of BmK M2 step by step in the process of refinement. In the first stages of refinement, the residues identical or similar to those in BmK M8 were defined. Then, judged by both the ($2F_o - F_c$) and the ($F_o - F_c$) electron-density maps, the residues differing from those in the BmK M8 sequence were gradually identified and substituted. When the electron densities did not fit the model well in the subsequent refinement, the residues were further changed to other likely residues. These residues were not defined until a good fit between the electron densities and the model was reached. Finally, detailed analysis of the stereochemical surroundings along with high-resolution electron-density maps allowed the discrimination between amide and acidic groups in Gln/Glu and Asn/Asp.

3. Results and discussion

3.1. Quality of the structure

The structure was refined to a resolution of 1.76 Å with a final R factor of 0.186 and an $R_{\rm free}$ of 0.248 for all data in the resolution range 20–1.76 Å. The results of refinement are summarized in Table 1. The terminal atom of even long flexible side chains could be found within the electron density contoured at 2.0σ in the omit $F_o - F_c$ map. The atomic positions of every residue were verified by the omit $F_o - F_c$ electron-density maps (Figs. 1–4). The Ramachandran plot (Ramachandran & Sasisekharan, 1968) shows that 88.5% of the non-glycine and non-proline residues fall in the core region; the remainder are in the allowed region. No residues were found in the generously allowed or disallowed regions. The upper limit of the error in the atomic positions is estimated to be between 0.20 and 0.25 Å by means of a Luzzati plot (Luzzati, 1952). In the whole structure, there is no residue with a mean main-chain B factor of more than 30 Å^2 or with a mean side-chain B factor of more

Table 1
Refinement statistics.

Resolution range (Å)	20.0–1.76
$I/\sigma(I)$ cutoff	None
Estimated errors in atomic positions (Å)	0.22
R_{work}	0.19
R_{free} (10% data)	0.25
R.m.s. deviations	
Bond length (Å)	0.015
Bond angles (°)	1.90
Dihedral angles (°)	26.85
Improper angles (°)	1.18
Ramachadran plot	
Core region (%)	88.5
Allowed region (%)	11.5
Protein model	
Protein atoms	504
Water molecules	87
Bound chloride (Cl^-)	1
Average temperature factors (Å^2)	
Protein	20.4
Main chain	18.8
Side chain	21.9
Water molecules	36.4
Chloride ion	9.4
Wilson B factor (Å^2)	22.0

than 45 Å^2. None of the 89 waters has a B factor of more than 55 Å^2.

3.2. The sequence determined by crystallographic analysis

The full sequence of 64 residues determined by the crystallographic analysis is as follows: Val-Arg-Asp-Ala-Tyr-Ile-Ala-Lys-Pro-His-Asn-Cys-Val-Tyr-Gly-Cys-Ala-Arg-Asn-Glu-Tyr-Cys-Asn-Asn-Leu-Cys-Thr-Lys-Asn-Gly-Ala-Lys-Ser-Gly-Tyr-Cys-Gln-Phe-Ser-Gly-Lys-Tyr-Gly-Asn-Gly-Cys-Trp-Cys-Ile-Glu-Leu-Pro-Asp-Asn-Val-Pro-Ile-Arg-Val-Pro-Gly-Lys-Cys-His.

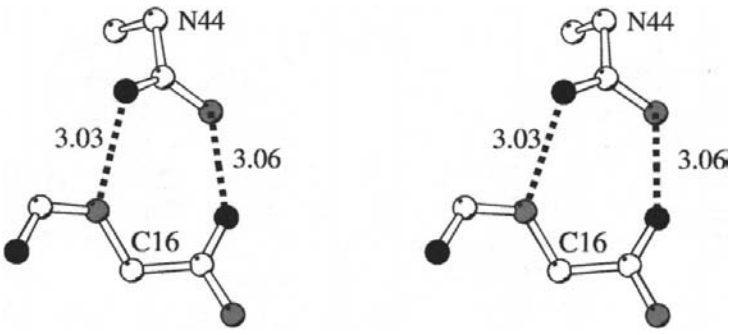

Figure 5
The hydrogen-bonding pattern involving the Asn44 side chain suggests that it has an amide group rather than an acidic group.

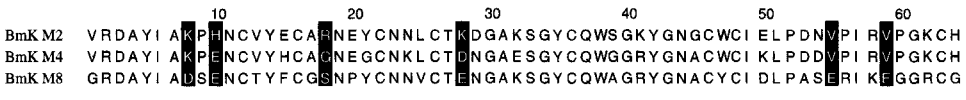

Figure 6
Sequence alignment of the basic BmK M2 with the neutral BmK M4 and the acidic BmK M8. The residues suggested to be related to the toxicity variance are highlighted.

The electron densities of all the residues in the final model are shown in Figs. 1–4. An example of the use of the hydrogen-bonding pattern in discriminating between amide and acid groups is illustrated in Fig. 5. The sequence alignment with the homologous proteins (Fig. 6) is consistent with the sequence determined crystallographically.

3.3. Main structural features

The overall folding of BmK M2 is similar to that of AaH II and BmK M8 (Housset *et al.*, 1994; Li *et al.*, 1996) as depicted in Fig. 7(*a*). A stretch of the α-helix (19–28) and a three-stranded sheet (2–5, 33–40, 43–50) form the scaffold of the molecular structure. Four disulfide bonds, Cys12–Cys63, Cys16–Cys36, Cys22–Cys46 and Cys26–Cys48, lock the secondary-structure elements tightly. Three loops protruding from the dense core of secondary structures constitute the flexible parts of the molecule.

The most striking feature of the structure of BmK M2 is a non-proline *cis* peptide bond found between residues 9 and 10 (Fig. 8). During refinement and model rebuilding it was impossible to restrain the ω value of the peptide bond 9–10 to $\pm180^\circ$, whereas the value moved easily towards 0° during rebuilding. The $2F_o - F_c$ and $F_o - F_c$ maps clearly show a *cis* conformation of the peptide bond between residues 9 and 10 (Fig. 8), with both the main chain and the side chain of residues 9 and 10 fitting the electron densities perfectly. In this *cis* peptide bond, the amide N atom is provided by a non-proline amino acid (His10). Therefore, it is a non-proline *cis* peptide bond. In proteins, non-proline *cis* peptide bonds occur only rarely, since the *trans* form is energetically more favourable than the *cis* form. In a thorough analysis (Stewart *et al.*, 1990), it was shown that only 0.05% of non-proline peptide bonds have a *cis* conformation. However, three BmK toxins, BmK M1, BmK M4 (He *et al.*, 1999) and BmK M2 (reported here), have been found to have a *cis* peptide bond. So far, five scorpion α-toxin structures, AaH II (Housset *et al.* 1994), BmK M8 (Li *et al.*, 1996), BmK M1, BmK M4 (He *et al.*, 1999) and BmK M2 (reported here), have been determined at high resolution. According to the new classification proposed by Gordon *et al.* (1996), AaH II and BmK M8 belong to the classical α-toxin group, but BmK M1, BmK M4 and BmK M2 belong to the group III α-like toxins. Interestingly, both AaH II and BmK M8 do not show any *cis* peptide bond in the structure, although BmK M8 has the same origin (the Chinese scorpion BmK) as BmK M1, BmK M4 and BmK M2. Therefore, the occurrence of the *cis* peptide bond 9–10 is more likely to be concerned with the group assignment than with the species assignment. Recently, Gordon *et al.* (1996) demonstrated that the α-like toxins have a different receptor-binding site in the sodium channel from the classical α-toxins. The result observed in BmK M2 further supports the suggestion

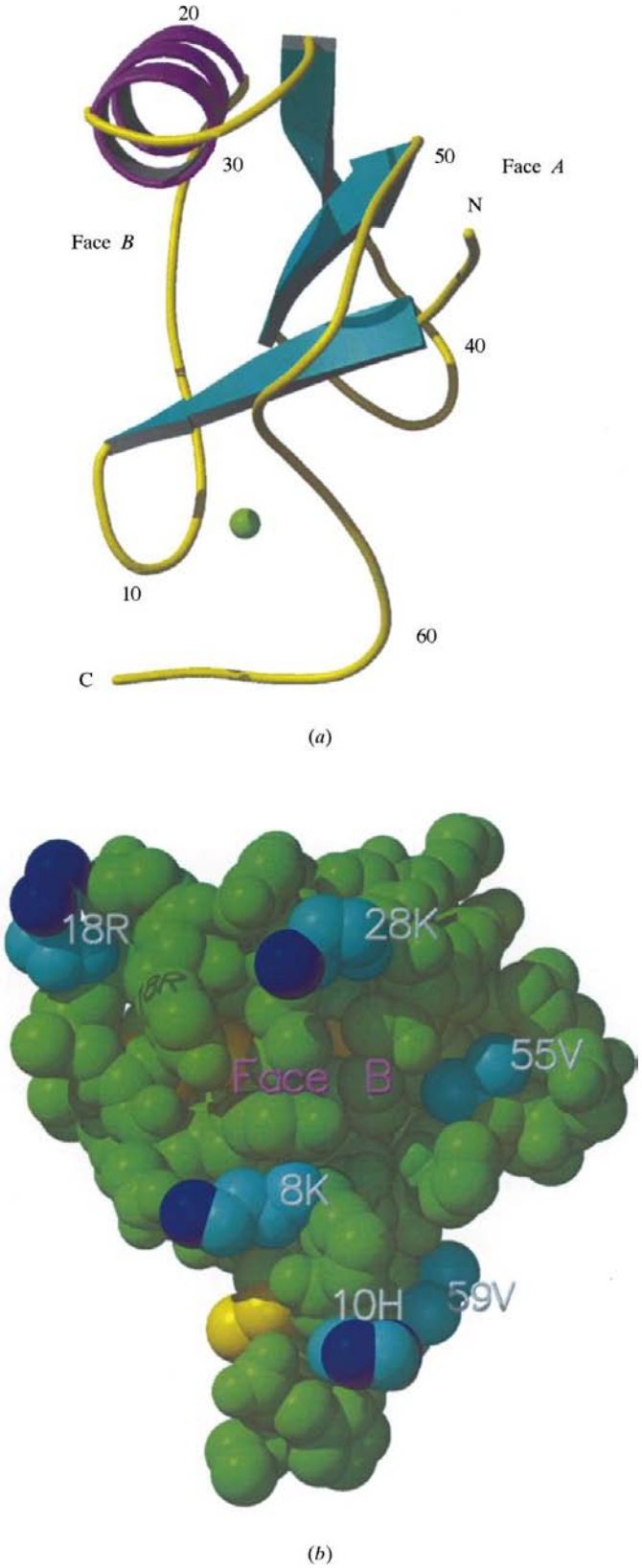

Figure 7
(*a*) The general fold of BmK M2. The bound Cl^- is depicted as a green ball. The opposite faces *A* and *B* are labelled. Face *A* is the conserved and hydrophobic face, while face *B* is variable. (*b*) CPK model of BmK M2. The side chains of the residues suggested to be involved in the changes in toxicity are highlighted in cyan (C atoms) and blue (N atoms) showing their positive electrostatic potential or neutral property.

that the unusual *cis* peptide bond between residues 9 and 10 is the common structural feature of the group III α-like toxins. However, a *cis* peptide bond has not been observed at this position in the scorpion toxins of other groups or families. This non-proline *cis* peptide bond has also not been observed in neurotoxins from other neurotoxic animals such as snakes, sea-anemones and spiders.

The major difference between the present structure and BmK M8 occurs at the turn 8–12 (containing the *cis* peptide bond) and the C-terminal segment 58–64 (Fig. 9), which had to be completely rebuilt. The differences in these two parts between the classical α-toxin (BmK M8) and the α-like toxin (BmK M2) may be related to the binding selectivity of the two kinds of toxins. Interestingly, these two parts are correlated in tertiary arrangement. Being energetically unfavourable, the *cis* peptide bond 9–10 is stabilized by two main-chain hydrogen bonds between residues 10 and 64 (Fig. 8). This implies that the spatial orientation of the C-terminus is correlated to the occurrence of the unusual *cis* peptide bond. The previous structural analysis (He *et al.*, 1999) of BmK M1 and BmK M4 showed a similar structural feature to that described above. Recently, Zilberberg *et al.* (1997) demonstrated by site-directed mutagenesis that both residues 10 and 64 are functionally important, playing direct roles in the toxin–receptor binding. Therefore, the *cis* peptide bond may be directly involved in the receptor binding. It is interesting that the formation of the functionally significant structural feature is mediated by a non-proline *cis* peptide bond, because it demonstrates a way to achieve a high level of molecular specificity and atomic precision through strained backbone geometry.

3.4. Residues possibly involved in the high toxicity of BmK M2

The toxic activity of BmK M2 is the strongest among the BmK mammalian neurotoxin series. The relative toxicity of BmK M2 (LD_{50} = 0.5 mg kg^{-1}) compared with the two weak toxins BmK M4 and BmK M8 are 8:1 and 20:1 (Li *et al.*, 1999), respectively. It is worth noting that the reduction of the toxic activity is accompanied by a lowering of the pI values, *i.e.* from 9.44 (BmK M2) to 7.53 (BmK M4) and 5.30 (BmK M8). Thus, the higher the pI value, the higher the toxicity. Sequence alignment of these three toxins is shown in Fig. 6. BmK M2 has 13 residues different from BmK M4 and 25 residues different from BmK M8. If we consider these homologous toxins as natural mutants arising from the divergence of the toxin gene, those substitutions that induce a change in the charge potential are probably most relevant to the changes of toxicity. Of particular interest are positions where the conserved or similar residues are found in the weak toxins BmK M4 and BmK M8 but not in BmK M2, or are not found in BmK M2 and BmK M4 but are found in the weakest toxin BmK M8. These residues, namely, 8, 10, 18, 28, 28, 55 and 59, are boxed in Fig. 6. These residues are all alkaline or neutral in BmK M2 but are neutral or acidic in the weaker BmK M4 and the weakest BmK M8. In their tertiary structures, these residues are mainly distributed on the molecular surface face *B* (Li *et al.*, 1996;

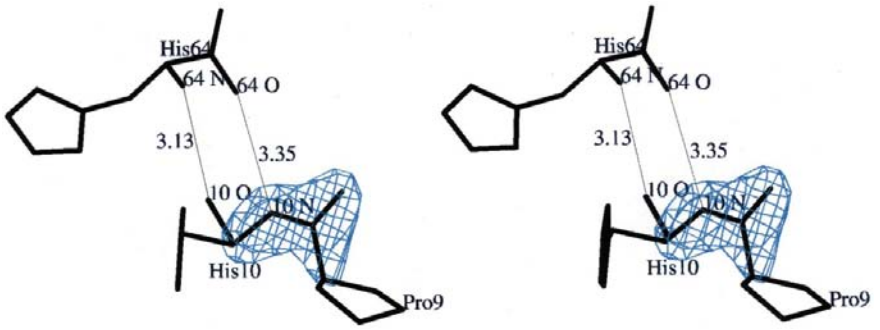

Figure 8
The omit $F_o - F_c$ electron-density map (contoured at 3.5σ) corresponding to the *cis* peptide group. His64 is also depicted in order to show its interaction with the *cis* peptide bond.

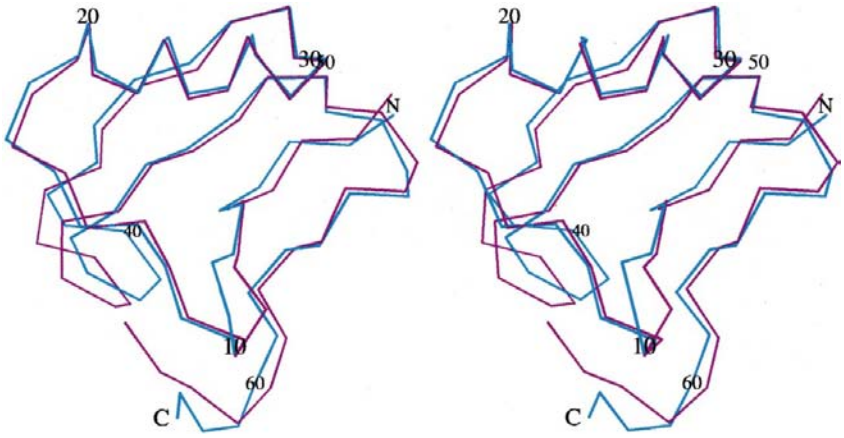

Figure 9
Comparison of the C^{α} trace of BmK M2 (cyan) with BmK M8 (purple). The orientation is similar to that in Fig. 7(*b*).

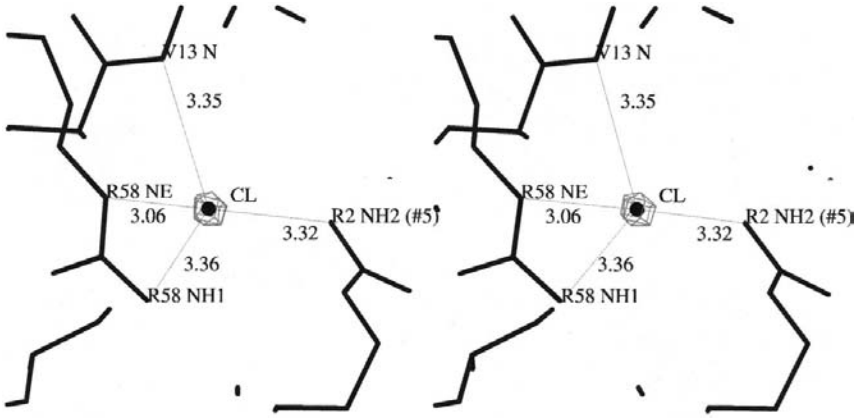

Figure 10
The environment of the bound Cl^- and the corresponding electron densities contoured at 5.0σ.

Fig. 7*b*). As a consequence, these mutations change the electrostatic potential of face *B* from negative or neutral, as in the weaker toxins BmK M4 and BmK M8, to positive, as in the stronger toxin BmK M2. This may be responsible for the high toxicity of BmK M2. The results obtained here thus further support the conclusion drawn from the structure analysis of BmK M8 (Li *et al.*, 1996).

3.5. Solvent molecules

A chlorine ion was found close to two arginine guanidyl groups. The high electron density at the corresponding position justified the identification (Fig. 10). The chlorine ion was excellently bonded, with four N atoms at suitable distances. It was suggested to play a key role in the crystal packing. Without this chlorine ion, the two guanidyl groups belonging to two neighbouring molecules could not be stabilized at such a short distance. The composition of the mother liquor used for growing the crystals suggested that the chlorine ion could come from the Tris–HCl buffer. The crystallization trials have also shown that crystals did not grow when HEPES–NaOH buffer was used instead of Tris–HCl buffer.

A total of 86 ordered water molecules were modelled. Most of them are bound to the surface of the protein. The packing interactions mostly involve salt bridges or hydrogen bonds. Intermolecular hydrogen bonds are formed either directly between protein atoms or through water molecules. Parts of the molecule directly involved in the crystal packing encompass the N-terminus (1–3), segment 18–20, segment 29–32 and residues 24, 37, 42, 54, 61 and 62.[1]

This work was supported by the Natural Science Foundation of China and the 863 High-Tech project. DCW is grateful to the Alexander von Humboldt Stiftung for short-term support. We thank Mr X.-D. Zhao of the National Biomacromolecular Laboratory for help in data collection.

References

Almassy, R. J., Fonticilla-Camps, J. C., Suddath, F. L & Bugg, C. E. (1983). *J. Mol. Biol.* **170**, 497–527.
Bernstein, F. C., Koetzle, T. F., Williams, G. J. B., Meyer, E. F. Jr, Brice, M. D., Rodgers, J. R., Kennard, O., Shimanouchi, T. & Tasumi, M. (1977). *J. Mol. Biol.* **112**, 535–542.
Brünger, A. T. (1990). *Acta Cryst.* A**46**, 46–57.
Brünger, A. T., Kuriyan, J. & Karplus, M. (1987). *Science*, **235**, 458–460.

[1] Supplementary material is available from the IUCr electronic archive (Reference: vj0023). Services for accessing this material are described at the back of this issue.

Couraud, F., Jover, E., Dobois, J. M. & Rochat, H. (1982). *Toxicon*, **20**, 9–16.
Deng, J.-P., Wang, M., Li, H.-M. & Wang, D.-C. (1996). *Chin. Biochem. J.* **12**, 603–607.
Dodson, E., Kleywegt, G. J. & Wilson, K. (1996). *Acta Cryst.* D**52**, 228–234.
Fontecilla-Camps, J. C., Habersetzer-Rochat, C. & Rochat, H. (1988). *Proc. Natl Acad. Sci. USA*, **85**, 7443–7447.
Gordon, D., Martineauclaire, M. F., Cestele, S., Kopeyan, C., Carlier, E., Benkhalifa, R., Pelhate, M. & Rochat, H. (1997). *J. Biol. Chem.* **271**, 8034–8045.
Gordon, D., Savarin, P., Gurevitz, M. & Zinn-Justin, S. (1998). *J. Toxicol. Toxin Rev.* **17**, 131–159.
He, X.-L., Li, H.-M., Zeng, Z.-H., Liu, X.-Q., Wang, M. & Wang, D.-C. (1999). *J. Mol. Biol.* **292**(1), 125–135.
Housset, D., Habersetzer-Rochat, C., Astier, J. & Fontecilla-Camps, J. C. (1994). *J. Mol. Biol.* **238**, 88–103.
Howard, A. J., Gilliland, G. L., Finzel, B. C., Poulos, T. L., Ohlendorf, D. H. & Salemme, F. R. (1987). *J. Appl. Cryst.* **20**, 383–387.
Hu, R.-Q., Wang, M., Lin, J.-L. & Lei, K.-J. (1989). *Zool. Res. Sinica*, **10**, 185–188.
Jin, L., Wang, M., Zeng, Z.-H., Hu, R.-Q. & Wang, D.-C. (1993). *Chin. Sci. Bull.* **38**, 561–563.
Kleywegt, G. J. & Brünger, A. T. (1996). *Structure*, **4**, 897–904.
Li, H.-M., Liu, Y.-S., Wang, M., Zhao, T. & Wang, D.-C. (1995). *Chin. Sci. Bull.* **40**, 746–748.
Li, H.-M., Wang, D.-C., Zeng, Z.-H., Jin, L. & Hu, R.-Q. (1996). *J. Mol. Biol.* **261**, 415–431.
Li, H.-M., Wang, M., Liu, Y.-S., Zhao, T., Jin, L. & Wang, D.-C. (1995). *Acta Biochem. Biophys. Sin.* **27**, 145–151.
Li, H.-M., Zhao, T., Jin, L., Wang, M., Zhang, Y. & Wang, D.-C. (1999). *Acta Cryst.* D**55**, 341–344.
Luo, M.-J., Xiong, Y.-M., Wang, M., Wang, D.-C. & Chi, C.-W. (1997). *Toxicon*, **35**, 723–728.
Luzzati, V. (1952). *Acta Cryst.* **5**, 802–810.
Ramachandran, G. N. & Sasisekharan, V. (1968). *Adv. Protein Chem.* **23**, 283–437.
Rochat, H., Benard, P. & Couraud, F. (1979). *Advances in Cytopharmacology*, Vol. 3, edited by B. Cecarelli & F. Clementi, pp. 325–334. New York: Raven Press.
Rossman, M. G. & Blow, D. M. (1962). *Acta Cryst.* **15**, 24–31.
Roussel, A., Fontecilla-Camps, J. C. & Cambillau, C. (1990). *Acta Cryst.* A**46**, C66–C67.
Stewart, D. E, Sarker, A. & Wampler, J. E. (1990). *J. Mol. Biol.* **214**, 253–260.
Watt, D. D. & Simard, J. M. (1984). *J. Toxicol. Toxin Rev.* **3**, 1 81–221.
Xiong, Y.-M., Ling, M.-H., Lan, Z.-D., Wang, D.-C. & Chi, C.-W. (1999). *Toxicon*, **37**, 335–341.
Xiong, Y.-M., Ling, M.-H., Wang, D.-C. & Chi, C.-W. (1997). *Toxicon*, **35**, 1025–1031.
Zhao, B., Carson, M., Ealick, S. E. & Bugg, C. E. (1992). *J. Mol. Biol.* **227**, 239–252.
Zilberberg, N., Froy, O., Loret, E., Cestele, S., Arad, D., Gordon, D. & Gurevitz, M. (1997). *J. Biol. Chem.* **272**, 14810–14816.